

# Impact of graph energy on a measurement of resilience for tipping points in complex systems

Christine M. Edwards<sup>1</sup>  | Roshanak Rose Nilchiani<sup>2</sup>  | Ian M. Miller<sup>3</sup>

<sup>1</sup>Lockheed Martin Corp, Highlands Ranch, Colorado, USA

<sup>2</sup>Stevens Institute of Technology, School of Systems and Enterprises, Hoboken, New Jersey, USA

<sup>3</sup>National Geographic Society, Washington, District of Columbia, USA

## Correspondence

Christine M. Edwards, Lockheed Martin Corp, 8740 Lucent Blvd., Highlands Ranch, Colorado 80129, USA.

Email: [christine.m.edwards@lmco.com](mailto:christine.m.edwards@lmco.com)

## Abstract

Societies depend on various complex and highly interconnected systems, leading to increasing interest in methods for managing the resilience of these complex systems and the risks associated with their disruption or failure. Identifying and localizing tipping points, or phase transitions, in complex systems is essential for predicting system behavior but a difficult challenge when there are many interacting elements. Systems may transition from stable to unstable at critical tipping-point thresholds and potentially collapse. One of the suggested approaches in literature is to measure a complex system's resilience to collapse by modeling the system as a network, reducing the network behavior to a simpler model, and then measuring the resulting model's stability. In particular, Gao and colleagues introduced a methodology in 2016 that introduces a resilience index to measure precariousness (the distance to tipping points). However, those mathematical reductions can cause information loss from reducing the topological complexity of the system. Herein, the authors introduce a new methodology that more-accurately predicts the location of tipping points in networked systems and their precariousness with respect to those tipping points by integrating two approaches: (1) a new measurement of a system's topological complexity using graph energy (created based on molecular orbital theory) and; (2) the resilience index method from Gao et al. This new approach is tested in three separate case studies involving ecosystem collapse, supply chain sustainability, and disruptive technology. Results show a shift in tipping-point locations correlated with graph energy. The authors present an equation that corrects errors introduced as a result of the model reduction, providing a measurement of precariousness that gives insight into how a complex system's topology affects the location of its tipping points.

## KEY WORDS

complexity theory, graph energy, phase transition, resilience, tipping point

## 1 | INTRODUCTION

So much depends upon the nature of tipping points in critical systems that must not fail. From power grids to food supply chains, from socioeconomic to ecological systems, modern societies rely on the continuous steady operation of the systems that support their needs. A tipping point is where a system transitions from one behavior to another, which is also called a phase transition when modeled mathematically. When a tipping point is reached, the system can become unstable and spiral into a different behavior pattern. This change can be beneficial or detrimental depending on the desired behavior of the system. Severe shifts in system behavior can lead to collapse. For example, in ecologies a tipping point can be triggered by or cause extinctions and lead to the complete collapse of the ecosystem. In supply chains, a tipping point can cause a sustainable supply chain to become overloaded and decimate supplies. In technology development, a tipping point could be a change in market dynamics due to a disruptive innovation or a new successful product.

To actively monitor the behavior of complex systems, their resilience can be measured. The challenge of accurately modeling the resilience of systems that have networked dynamics is common to economics, biology, ecology, chemistry, physics, and engineering<sup>1–3</sup> and is essential in predicting risk.<sup>4</sup> In the field of ecology, a measurement of resilience is the magnitude of disturbance that can be absorbed before the system changes its behavior, which has led other fields to refer to this measurement as ecological resilience.<sup>5</sup> One approach to measuring ecological resilience is precariousness, which is the distance from a system's current operational state to the nearest tipping point.<sup>6</sup> Resilience engineering as a framework<sup>7</sup> incorporates ecological resilience and precariousness along with other metrics more-traditionally considered in engineering. Those metrics include the time to recovery, the performance decline during a disturbance, and the recovered performance after a disturbance.<sup>8</sup> Figure 1(A) illustrates the concept of precariousness. When a system is perturbed away from its nominal operating zone and moves closer to a tipping point, its precariousness decreases. In cases where critical system behavior needs to be sustained, measuring precariousness can provide system managers, designers, and stakeholders with information on how to avoid approaching undesired

tipping points. In cases where a tipping point is desired, measuring precariousness can provide insight into how to change the system to achieve that change in behavior.

Until recently, estimating resilience relied on low-dimensional models, which are models reduced to lower dimensions from higher dimensional data, such as networks with limited numbers of nodes or layers,<sup>9,10</sup> that did not adequately capture the complexity of the system.<sup>11</sup> In 2016, a revolutionary resilience index was introduced by Gao and colleagues through a paper published in *Nature*.<sup>11</sup> This first-of-a-kind approach uses a new mathematical dimension, named the effective plane, to show how close a complex system is to its tipping points. In this effective plane illustrated in Figure 1(B), a resilience index is defined,  $\beta_{\text{eff}}$ , which can be used to calculate a system's precariousness to a tipping point by identifying the location of the tipping point,  $\beta_{\text{eff}}^c$ , and measuring precariousness with  $\beta_{\text{eff}} - \beta_{\text{eff}}^c$ . To use this approach, the system is first modeled as a network in which dynamics equations guide the behavior of each node. These equations are translated into the effective plane with an operator that essentially averages the impact of each node on other nodes, which flattens the model into one dynamics equation. One fascinating aspect of the effective plane is that the behavior of large complex networks is reduced to that of a simpler system that has only one or several tipping points. The resulting model enables a measurement of precariousness for large networks, but it also loses some of its structure and the complex dynamics in that topology. We theorize that there is an impact from this loss of topological complexity in this model reduction, and if we can measure and adjust for that topological complexity, then we could improve the prediction of tipping points in large complex systems using this new method.

To begin, we theorize that when large-scale systems are modeled as networks where each node has similar dynamics, their modeled structure can be similar to that of molecular systems and interactions, and their levels of structural complexity can be measured using adjacent methods from molecular science. For example, researchers in complexity theory and systems engineering<sup>12,13</sup> have correlated the topological complexity of systems with graph energy ( $E$ ), including the visualization shown in Figure 2(A) that shows how different

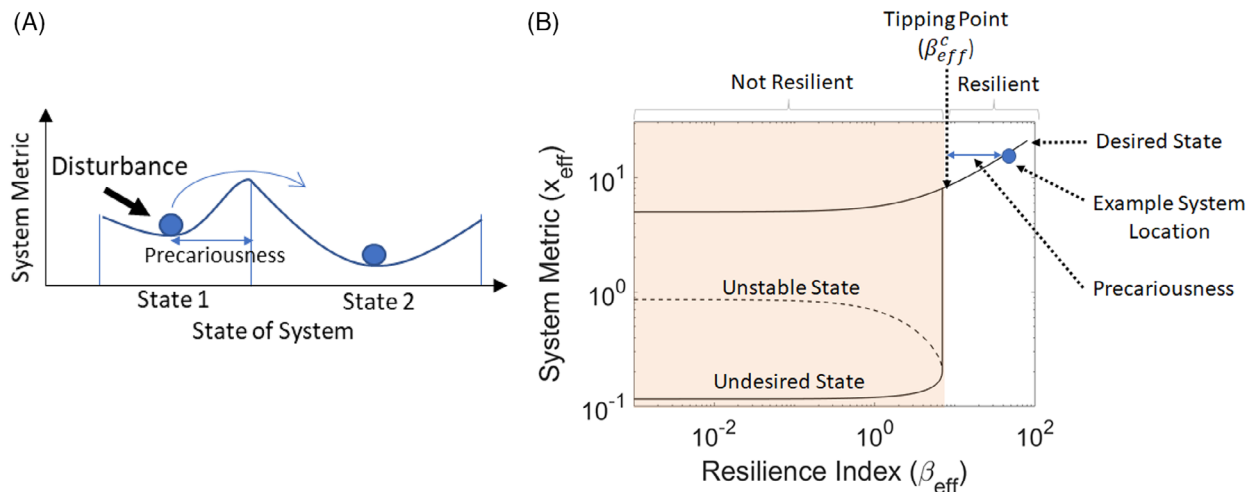


**FIGURE 1** Precariousness as an illustrated concept (A) and as a measurement in the effective plane (B).

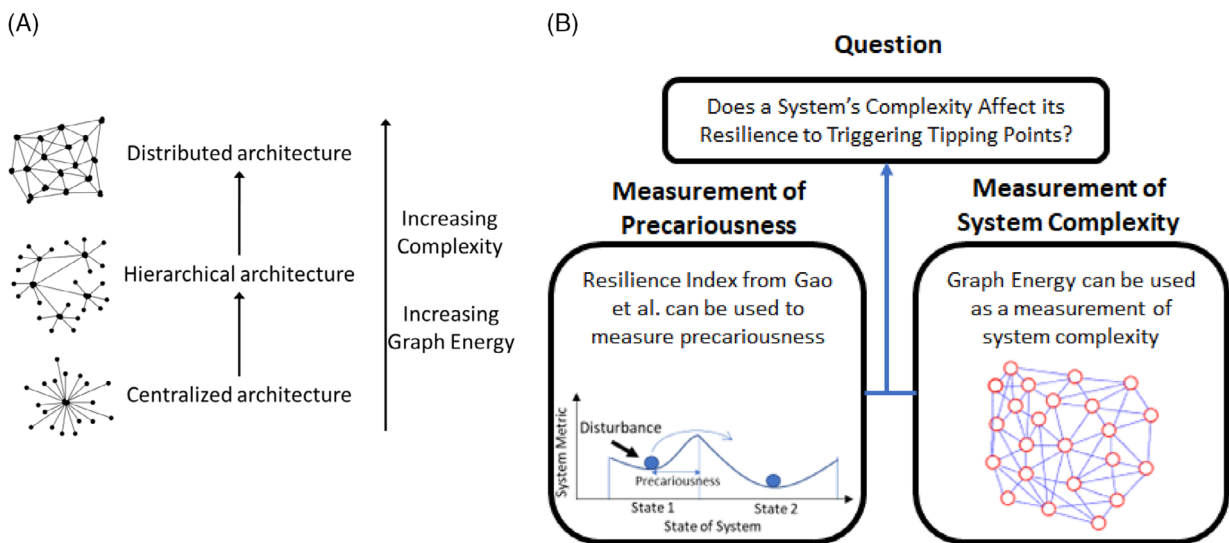


**FIGURE 2** Graph energy as an illustrated concept (A) redrawn from,<sup>12</sup> and approach of applying resilience index and graph energy to investigate research question (B).

topological patterns relate to graph-energy levels. Graph energy was originally a topological measurement for molecules.<sup>14–17</sup> The origin of graph energy was a measurement of binding energy in Hückel molecular orbital (HMO) theory, which quantifies total  $\pi$ -electron energy.<sup>18</sup> The calculation of the energy of the system in HMO theory has a similar form as the equations used by Gao et al. to model complex system dynamics, but with graph energy as an additional adjustment. This similarity led to the question of whether graph energy could provide a similar adjustment to the resilience-index method of Gao et al. Intriguingly, graph energy was shown to correlate with phase transition/tipping-point behaviors in chemistry and biology,<sup>19</sup> including thermodynamic properties and resonance stabilization of organic molecules.<sup>20,21</sup> It also correlates with quantitative structure–activity relationship (QSAR) models,<sup>22,23</sup> entropy,<sup>24,25</sup> and properties of proteins.<sup>26,27</sup> Hypothesizing that graph energy could provide similar insight into the impact of system complexity on tipping points in large-scale systems, we adapt molecular orbital theory in the context of graph energy to estimate a system's topological complexity.

Ultimately, we seek insight into the larger fundamental question: does the complexity of a system affect its resilience to triggering tipping points? To gain insight into this larger question, the research questions are: (1) does graph energy (as a measurement of topological complexity) affect the accuracy of the resilience index (as a measurement of precariousness), and (2) can topological complexity's impact be measured and integrated into the resilience-index method? This research explores these questions by first discussing the previous work that this research builds on in measuring system complexity and resilience to triggering tipping points. Then, the equations for graph energy are adapted to become a measurement for system complexity and integrate into the resilience-index approach from Gao et al. that measures a system's precariousness to tipping points. The combination of these methods is illustrated in Figure 2(B). These methods are then tested in three case studies of systems undergoing tipping points, to assess the impact of the system's complexity on the system's precariousness.

## 2 | LITERATURE REVIEW

### 2.1 | Measuring system complexity

Complex nonlinear systems make up many of the systems that our society depends on today. One definition is that complexity is the degree of difficulty in accurately predicting future behavior of a system.<sup>28–30</sup> The MIT Engineering Systems Division defined a complex system as a system “with components and interconnections, interactions, or interdependencies that are difficult to describe, understand, predict, manage, design, or change. It includes dynamic, static, and structural aspects<sup>31</sup> Other attributes that make a system complex include nonlinearity, nonequilibrium dynamics, and interrelated dynamics,<sup>28,32,33</sup> leading to tipping points that are difficult to predict.

For measuring complexity, many sources of quantitative complexity measures from literature focus on structural, dynamic, organizational, and information/computational complexity.<sup>34,35</sup> Because the approach of this research Models a system with a graph representation and reduces the system content using weighted sums, the most relevant complexity measures from the literature are those that use similar graph representations and reductions. Complexity metrics with these characteristics include those derived from entropy<sup>35–38</sup> and cyclomatic complexity.<sup>39</sup> Out of these reviews of complexity metrics, graph energy was selected because of: (1) previous research showing its use as a measurement of topological complexity in systems engineering, discussed below; (2) its history of providing insight into tipping-point behavior in molecular systems, as discussed in Section 1; (3) potential to be integrated with method from Gao et al. due to its similar mathematical form, as shown in Section 3.

The origin of graph energy was an equation derived by Hückel in 1931 to measure the electron energy for a certain class of organic molecules.<sup>18</sup> The theory was expanded by Graovac, Gutman, and Trinajstić using graph theory.<sup>14</sup> The graph-theory form of Hückel's molecular orbital theory (HMO) measures the absolute energy levels ( $\epsilon_i$ ) of the  $i$ -th molecular orbit were related to the eigenvalues ( $\lambda_i$ ) of the adjacency

matrix ( $\mathbf{A}$ ) of the molecular graph ( $G$ ) using Equation (1). The other terms are total  $\pi$ -electron energy ( $\varepsilon_\pi$ ), number of vertices of the underlying molecular graph ( $n$ ), the Coulomb integral pertaining to a carbon atom ( $\alpha$ ), and the carbon-carbon resonance integral ( $\beta$ ).

$$\varepsilon_\pi = \sum_{i=1}^n n\varepsilon_i = n\alpha + n\beta \sum_{i=1}^n |\lambda_i| \quad (1)$$

The energy of a graph, or the graph energy ( $E$ ), was initially represented as  $E = \sum_{i=1}^n |\lambda_i|$ , so that Equation (1) became  $\varepsilon_\pi = n\alpha + n\beta E$ . Nikiforov extended this theory to any matrix by replacing the eigenvalues with singular values.<sup>40</sup> The resulting graph energy is represented by Equation (2), where  $\sum_{i=1}^n \sigma_i$  is the sum of the singular values of a graph's binary adjacency matrix,  $A^{binary}$ .

$$E = \sum_{i=1}^n \sigma_i \quad (2)$$

The graph-energy concept was adapted by Sinha, Suh, and de Weck to measure the structural complexity,  $C$ , of a system using Equation (3).<sup>12</sup> In this equation, the complexity contributions are summed for each component  $i$ , with  $\alpha_i$  representing a measurement of the complexity of each component,  $\beta_{ij}$  representing a measurement of the complexity of the interface between components  $i$  and  $j$ ,  $A^{binary}$  is a binary adjacency matrix of the graph with  $A_{ij}^{binary} = 1$  when there is an edge between components  $i$  and  $j$  and 0 otherwise,  $\gamma$  as a scaling factor, and  $E$  as the graph energy using Equation (2). Note how  $\beta_{ij}$  in Equation (3) has a similar purpose as  $\beta$  in Equation (1) as a modifier, but it is no longer a constant and is allowed to vary as a matrix entry. Sinha, Suh, and de Weck's research showed that the structure of the system was more centralized with low graph energy,  $E$ , and became more distributed with higher  $E$  as shown earlier in Figure 2(A). They also showed how systems that were more distributed with higher  $E$  were more complex than systems with lower  $E$  using other complexity measurements.

$$C(n, m, A) = \sum_{i=1}^n \alpha_i + \left( \sum_{j=1}^m \sum_{i=1}^n \beta_{ij} A_{ij}^{binary} \right) \gamma E \quad (3)$$

Building from the previous work of Sinha, Suh, and de Weck, which showed that graph energy can be used as a measure of topological complexity for systems, the research in this paper implements graph energy to determine how topological complexity affects resilience to triggering tipping points, or precariousness.

## 2.2 | Measuring resilience to triggering tipping points

In the engineering domain, one definition of resilience from IEEE Technical Report PES-TR65 and FERC Docket No. AD18-7-000 is "the ability to withstand and reduce the magnitude and/or duration of disruptive events, which includes the capability to anticipate, absorb, adapt to, and/or rapidly recover from such an event".<sup>41,42</sup> One type of metric that can be incorporated into resilience management is the magnitude of disturbance the system can absorb before it's steady-

state shifts to a new equilibrium.<sup>43</sup> This type of resilience metric is used frequently in ecology research, leading to some articles naming it "ecological resilience".<sup>44,45</sup>

In 2022, Dakos and Kéfi performed a review of ecological resilience metrics.<sup>46</sup> They outlined the common approach of mathematically modeling the stability landscape of a system using graphs similar to those in Figure 3. The stability landscape is a graph where the basins (minima) are the stability points where a system can reach a stable state, and the saddle points are where a system will tip from being attracted towards one stability point to another. One of the metrics they list is the distance to the saddle point, referred to as precariousness,<sup>6</sup> which aligns with the definitions of precariousness discussed above. One of their identified weaknesses for this approach is that it uses low-dimensional models, which are models that are reduced to a lower dimension from higher dimensional data. For example, Figure 1(A) shows what they call a one-dimensional stability landscape, in that it graphs the stability landscape for only one variable. Low dimensional models like Figure 3(A) are often approximating a more-complex reality, but they can still provide insight by enabling calculation of metrics like precariousness. Research that has advanced ecological-resilience models with more dimensions includes methods in constructing two-dimensional and higher stability landscapes.<sup>47</sup> A two-dimensional stability landscape is illustrated in Figure 3(B). However, some research in higher-dimensional models have been unable to derive stability points and saddle points as the system model becomes more complex.<sup>48</sup>

Another method for modeling tipping points is with phase transitions.<sup>49</sup> Phase transitions occur when a system "tips" from one state of behavior into another state of behavior. The measurement of tipping points has been advanced by Sole<sup>50</sup> and van Voorn<sup>51</sup> in the categorization of types of tipping points, illustrated in Figure 4. A bifurcation, or first-order phase transition, occurs when the stable steady-state transitions to an unstable state, shown as a dashed line. A separatrix, or second-order phase transition, is when the state of a system crosses a boundary that causes two possible states. The case studies that were selected for this research are bifurcation phase transitions, where the systems begin with a stable initial state, but then can cross a threshold where they can either continue to operate in a stable state or become unstable.

The method introduced by Gao et al. enables modeling a system with many dimensions (e.g., a networked system with thousands of nodes). Like the approaches from the review by Dakos and Kéfi,<sup>46</sup> this method reduces high-dimensional data to one or two dimensions so that low-dimensional resilience metrics like precariousness can be calculated. However, the strength of this method is that the translation into the effective plane using the resilience index,  $\beta_{eff}$ , maintains some of the complexity of the high-dimensional data by essentially averaging the impact each node has on other nodes. Even though this  $\beta_{eff}$  reduction captures the impact of nodes on each other, it still loses some of the complexity of the larger structure, which is a weakness of this method under investigation in this paper. Another weakness of this method is it requires representing systems as networks with similar dynamics at each node. As a result, the randomness of individual components and behaviors of a complex system are not captured with this approach.

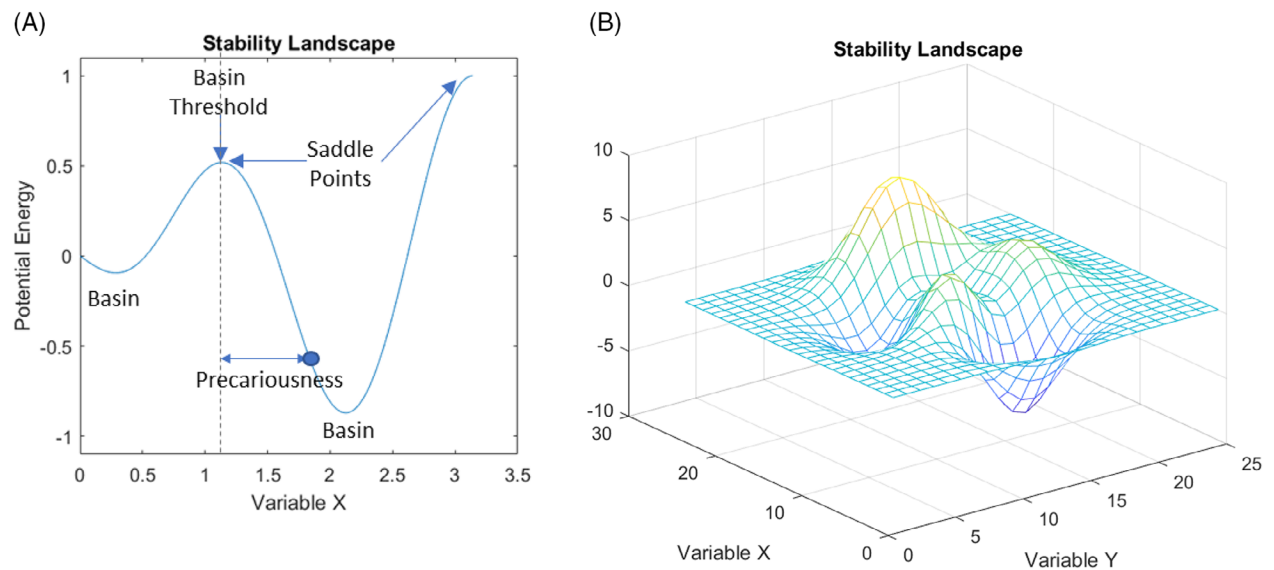


**FIGURE 3** Hypothetical stability landscapes that are referred to as one-dimensional (A) and two-dimensional (B).

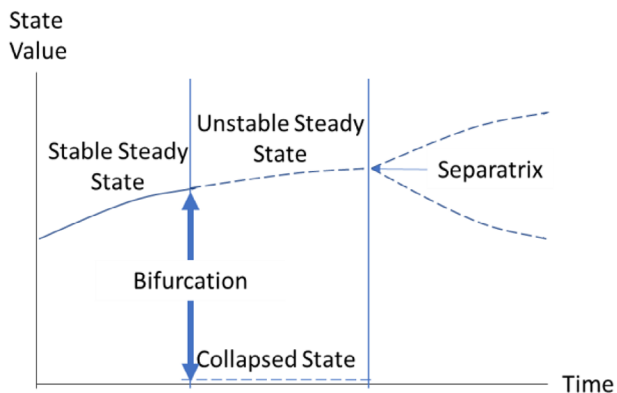


**FIGURE 4** Diagram depicting bifurcation and separatrix tipping points, redrawn from ref. 50.

The research that has been built on Gao et al. mostly includes investigating the practical application of their method, for example, refs. 52–54 or comparing other methods or models for measuring large network stability or resilience, for example, refs. 55, 56. Few works directly use and expand on this resilience index method. They include a model that expands on the mutualistic ecological model used by Gao et al. to include predator-prey dynamics<sup>57</sup> and an investigation of the assumptions and limitations of the method.<sup>58</sup> The following research is the first to investigate the impact of graph energy on this resilience index method.

### 3 | METHOD FOR ASSESSING THE IMPACT OF GRAPH ENERGY ON RESILIENCE TO TIPPING POINTS

As introduced in Section 1, the overarching question for this research is: “does a system’s complexity impact its resilience to triggering tipping

points?” The approach selected for this research was to investigate how system topological complexity, as measured by graph energy, impacts a system’s resilience to tipping points, as measured by the resilience index from Gao et al. The method used to explore this problem is to repeat the method used by Gao’s research group in the development and validation of their resilience index, but adding an assessment of how the system’s graph energy, used as a measure of topological complexity, impacts or perhaps moves the location or nature of tipping points calculated by the resilience index, and applying the new combined method to three case studies.

The method developed by Gao et al.<sup>11</sup> starts with a network-based dynamics model of a system. Each node,  $i$ , has a differential equation for  $\frac{dx_i}{dt}$  that describes the behavior of the system. In this equation,  $F(x_i)$  models the self-dynamics of the node, and  $G(x_i, x_j)$  models the effect of node  $i$  on node  $j$ , which is summed over  $N$  nodes. The adjacency matrix,  $A$ , is weighted so that each element,  $A_{ij}$ , captures the impact that node  $j$  has on the dynamics of node  $i$ .

$$\frac{dx_i}{dt} = F(x_i) + \sum_{j=1}^N A_{ij} G(x_i, x_j) \quad (4)$$

This set of dynamics equations is translated into the effective plane using the following conversion.

$$\beta_{\text{eff}} = \frac{\mathbf{1}^T \mathbf{A} s^{in}}{\mathbf{1}^T \mathbf{A} \mathbf{1}} \quad (5)$$

$$x_{\text{eff}} = \frac{\mathbf{1}^T \mathbf{A} \mathbf{x}}{\mathbf{1}^T \mathbf{A} \mathbf{1}} \quad (6)$$

For Equations (5) and (6),  $\mathbf{1}$  is the unit vector  $\mathbf{1} = (1, \dots, 1)^T$ ,  $\mathbf{x} = (x_1, \dots, x_N)^T$ , and  $s^{in} = (s_1^{in}, \dots, s_N^{in})^T$  is the vector of incoming weighted degrees in adjacency matrix  $\mathbf{A}$ , with  $s_i^{in} = \sum_{j=1}^N A_{ij}$ .

$\beta_{\text{eff}}$  becomes a scalar that is essentially a measurement of the incoming weighted degree averaged across the network. Conceptually, it measures how connected the network is by averaging the impact the

network nodes have on each other. The dynamic variable  $x_{\text{eff}}$  portrays a combined description of the dynamics of the system in the effective plane. Through this conversion, the set of  $N$  number of differential equations is reduced to one differential equation.

$$\frac{dx_{\text{eff}}}{dt} = F(x_{\text{eff}}) + \beta_{\text{eff}} G(x_{\text{eff}}, x_{\text{eff}}) \quad (7)$$

The tipping points of the system are found by solving for the stability points of Equation (7). The critical resilience index located at those stability points is  $\beta_{\text{eff}}^c$ . A system's distance to its tipping points is measured by calculating its current  $\beta_{\text{eff}}$  and how far it is from  $\beta_{\text{eff}}^c$ . With this approach,  $\beta_{\text{eff}} - \beta_{\text{eff}}^c$  becomes a measurement of precariousness, as illustrated in Figure 1(B).

Note how graph theory and the effective plane use different kinds of adjacency matrices, with the former implementing a binary adjacency matrix ( $A^{\text{binary}}$ ) and the latter implementing a weighted adjacency matrix ( $A$ ). To better understand how to combine these methods, the graph energy Equations (1)–(3) are adapted into Equations (8) and (9), where the energy contribution of each element  $i$  ( $\varepsilon_i$ ) includes the internal energy of each element,  $\alpha_i$ , the energy of each connection,  $\beta_{ij}$ , and the graph-energy adjustment for topology of the system,  $E$ .

$$\varepsilon_i = \alpha_i + \sum_{j=1}^N A_{ij}^{\text{binary}} \beta_{ij} E \quad (8)$$

As discussed in Section 2, the graph energy,  $E$ , is the sum of the singular values,  $\sigma_i$ , of the binary (0,1) adjacency matrix  $A^{\text{binary}}$  using Equation (9).

$$E = \sum_{i=1}^n \sigma_i \quad (9)$$

A new term introduced here, effective system energy,  $\varepsilon_{\text{eff}}$ , can be calculated by translating Equation (8) into the effective plane using  $\varepsilon_{\text{eff}} = \frac{1^T A \varepsilon}{1^T A 1}$ ,  $\alpha_{\text{eff}} = \frac{1^T A \alpha}{1^T A 1}$ , and  $\beta_{\text{eff}} = \frac{1^T A s^{in}}{1^T A 1}$ . However, to use these translation equations, the adjacency matrix  $A$  needs to be weighted. The relationship between the elements of the weighted adjacency matrix,  $A_{ij}$ , and the elements of the binary adjacency matrix,  $A_{ij,\text{binary}}$ , is established with Equation (10), such that Equation (8) becomes Equation (11).

$$A_{ij} = A_{ij,\text{binary}} \beta_{ij} \quad (10)$$

$$\varepsilon_i = \alpha_i + \sum_{j=1}^N A_{ij} E \quad (11)$$

Then remarkably, when Equation (11) is translated into the effective plane, that weighted adjacency matrix that has the  $\beta_{ij}$  elements reduces to the resilience index,  $\beta_{\text{eff}}$ , as shown in Equation (12).

$$\varepsilon_{\text{eff}} = \alpha_{\text{eff}} + \beta_{\text{eff}} E \quad (12)$$

This resulting equation provides insight into how graph energy,  $E$ , can be adjacently applied to systems in other fields. Conceptually, the right side of this effective system energy,  $\varepsilon_{\text{eff}}$ , equation can be understood as a measurement of the energy stored in the structure of the

connections between the elements of a system. For example, when it is applied to an ecosystem model, it represents the topological structure in the interactions between species. One of the effects of the effective plane is that the system's model loses information about the system's topological structure, and the nuances in the dynamics caused by that structure. The research in this paper predicts that the measurement of graph energy can be used to assess the impact of reduced topological complexity in the system.

## 4 | CASE STUDIES, RESULTS, AND DISCUSSIONS

Three use cases were simulated to assess the relationship between energy and the resilience index calculated with these methods. The first case study builds on the ecological analysis performed by Gao et al. by adding an assessment of how graph energy impacts their method. The second case study analyzes a supply chain model, to show that these combined methods are extensible to managing tipping points in other kinds of systems that include engineered systems. The third case study assesses a tipping point when a disruptive technology takes over a market. The translation of these case studies into the effective plane and the calculation of their tipping points are in references.<sup>11,65–67</sup> For each case study, the MATLAB script  $A^{\text{binary}} = \text{binary}(A)$  was used to calculate the binary adjacency matrix from each of the weighted adjacency matrices. Then the graph energy,  $E$ , was calculated with Equation (9) by summing the singular values of  $A^{\text{binary}}$ .

### 4.1 | Case study 1: Mutualistic ecosystem model

The ecological case studies in Gao et al.<sup>11</sup> were repeated, but with calculation of the graph energy,  $E(A^{\text{binary}})$ , of each ecosystem. The dynamics were simulated using the following equation for dynamics in species populations in ecosystems with mutualistic interactions between species:

$$\frac{dx_i}{dt} = B_i + x_i \left( 1 - \frac{x_i}{K_i} \right) \left( \frac{x_i}{C_i} - 1 \right) + \sum_{j=1}^N A_{ij} \frac{x_i x_j}{D_i + E_i x_i + H_j x_j} \quad (13)$$

The first term,  $B_i$ , is the migration rate. The second term describes the growth of the species,  $x_i$ , due to Allee effect and migration, with  $C$  as the Allee constant, and  $K$  as the environment carrying capacity. The third term models the interaction between species  $i$  and  $j$ , with the parameters  $D$ ,  $E$ , and  $H$  used to saturate that part of the function when populations are large. For the ecosystem case studies, these parameters were set equal to the same values as Gao et al., with  $B_i = B = 0.1$ ,  $C_i = C = 1$ ,  $K_i = K = 5$ ,  $D_i = D = 5$ ,  $E_i = E = 0.9$ , and  $H_j = H = 0.1$ .

Following Gao et al., the dynamics equation is recast in terms of the effective plane:

$$\frac{dx_{\text{eff}}}{dt} = B + x_{\text{eff}} \left( 1 - \frac{x_{\text{eff}}}{K} \right) \left( \frac{x_{\text{eff}}}{C} - 1 \right) + \beta_{\text{eff}} \frac{x_{\text{eff}}^2}{D + (E + H)x_{\text{eff}}} \quad (14)$$

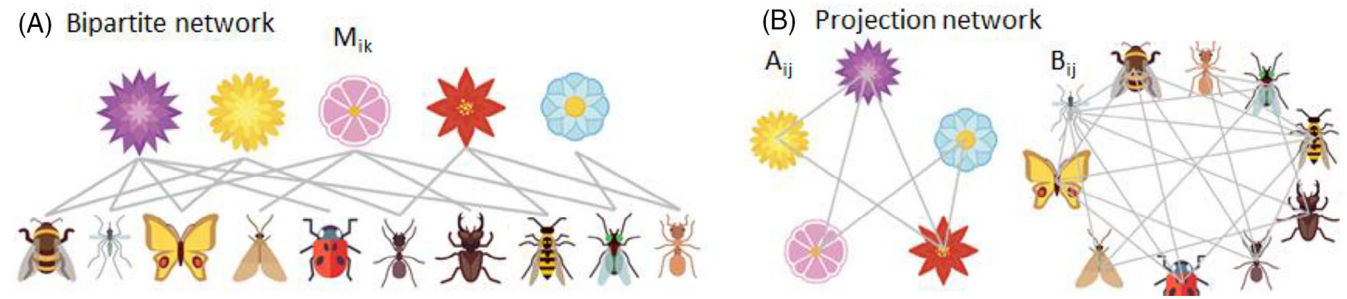


**FIGURE 5** Diagram depicting bipartite network (A) and projection network (B), redrawn from.<sup>11</sup>

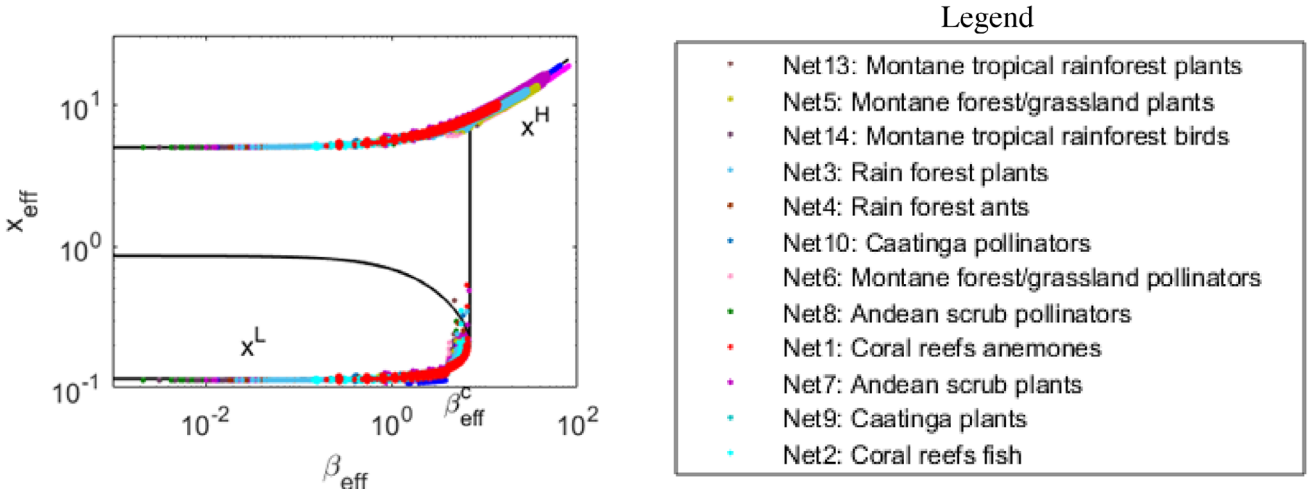


**FIGURE 6** Simulation results, redrawn from ref. 11.

where  $\beta_{\text{eff}}$  is the resilience index and  $x_{\text{eff}}$  shows population health. The stability points for this equation are found by setting Equation (14) and the partial derivative of Equation (14) equal to zero and solving for  $\beta_{\text{eff}}$ , resulting in a predicted bifurcation at  $\beta_{\text{eff}}^c = 6.97$ . For the case study, adjacency matrices were formed to describe species interactions in six real ecosystems that have mutualistic behavior between two kinds of species. The data sources (listed in the supplemental for Gao et al.<sup>11</sup>) first had the data captured in the form of bipartite networks illustrated in Figure 5(A), which show which species rely on each other with matrix elements  $M_{ij}$ . The weighted adjacency matrices for Equation (13) were formed by creating projection networks of those bipartite networks as illustrated in Figure 5(B) using  $A_{ij} = \sum_{k=1}^m \frac{M_{ik}M_{jk}}{\sum_{s=1}^n M_{sk}}$ , which are input into Equation (13) as  $A_{ij}$ .

The model was validated through simulation in Gao et al.,<sup>11</sup> which uses a fourth-order Runge–Kutta stepper (MATLAB function `ode45`). Figure 6, shows the data from their simulations plotted over Figure 1(A). A healthy ecosystem begins on a point along line  $x^H$ , with a high number of species captured in the state parameter  $x_{\text{eff}}$ . As the modeled ecosystem is weakened, the resilience index,  $\beta_{\text{eff}}$ , drops and eventually reaches the critical threshold at  $\beta_{\text{eff}}^c = 6.97$ . Below this threshold, the ecosystem can become unstable and drop to the  $x^L$  line, which means that the ecosystem completely collapsed to zero population. The difference between  $\beta_{\text{eff}}$  and  $\beta_{\text{eff}}^c$  can be used as a measurement

of precariousness. When the resilience index  $\beta_{\text{eff}}$  reaches  $\beta_{\text{eff}}^c$ , the system can trigger a tipping point. Further details on these data sources, model setup, and model validation can be found in the supplemental for Gao et al.<sup>11</sup>

The simulation was adapted to also calculate graph energy using Equation (9). While monitoring graph energy scaled by network size,  $E/N$ , where  $N$  is the number of nodes, the ecosystems were perturbed by randomly removing network nodes and edges. To simulate species extinction, a node was removed by deleting a row or column of the adjacency matrix. In this case, both the graph energy and  $\beta_{\text{eff}}$  decrease (Figure 7A). To simulate ecological (e.g., geographic) separation, an edge between species was removed without necessarily causing species extinction, and the  $\beta_{\text{eff}}$  decreases, but the graph energy initially increases. (Figure 7B). After many ecological separations, the ecosystem is so weakened that it has few interspecies connections left. At this point, every subsequent separation causes cascading extinctions in species as they lose their mutualistic support. Both the graph energy and  $\beta_{\text{eff}}$  values decrease and the ecosystem collapses. Each simulation repeated randomized node or edge removals until the resulting adjacency matrix was too small to support the Runge–Kutta stepper. For each iteration on the adjacency matrix, the species interaction was simulated to determine if the ecosystem sustained itself or collapsed to zero population (labeled with black asterisk \*, Figure 7C). Color dots

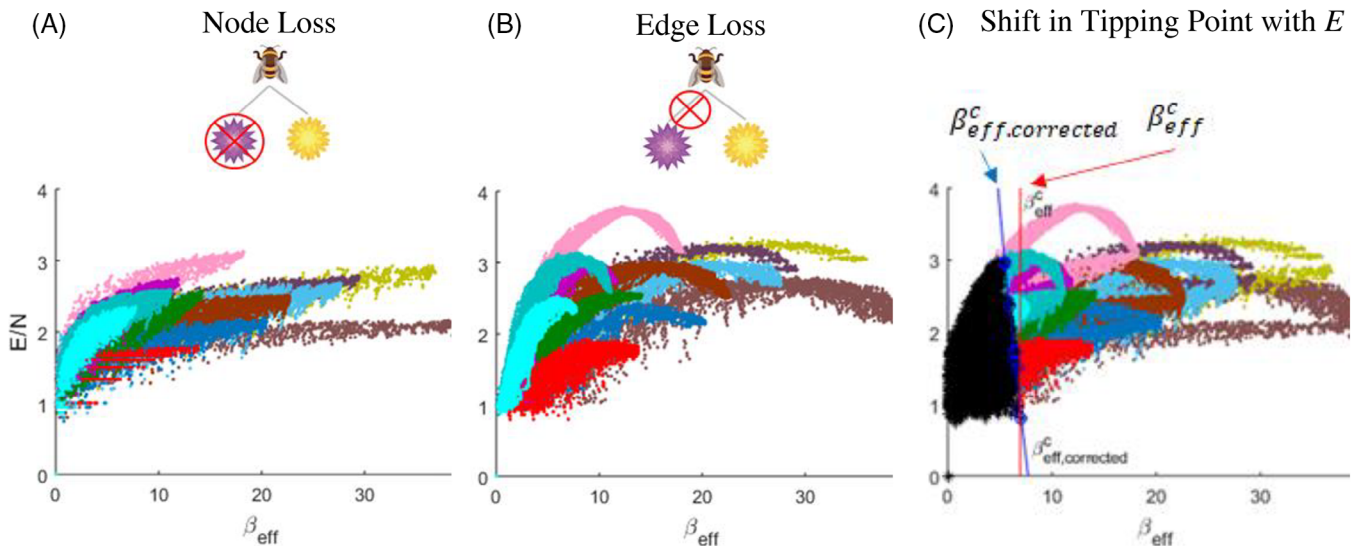


**FIGURE 7** Graph energy versus  $\beta_{\text{eff}}$  patterns with node loss (A), edge loss (B), and combined (C) using legend from Figure 6, ecosystem collapses labeled with black \*, predicted tipping point at  $\beta_{\text{eff}}^c = 6.97$ , and observed shift in actual tipping point  $\beta_{\text{eff},\text{corrected}}^c$ .

show results of 50–100 simulation runs for each ecosystem network using the legend in Figure 6.

Results show that for systems with higher graph energy, the ecosystems did not start collapsing at  $\beta_{\text{eff}}^c = 6.97$ , as predicted by Gao et al., but weakened further into a lower  $\beta_{\text{eff}}$  region and instead started collapsing along the  $\beta_{\text{eff},\text{corrected}}^c$  line shown in Figure 7(C). Using Figure 2(A) as a reference, the ecosystems with a higher  $E$  are more distributed in their topology, such that in the mutualistic ecosystem simulation they would likely maintain more supportive connections between species than a more-centralized lower  $E$  ecosystem, which would have fewer supportive connections between species. As a result, the ecosystems with higher  $E$  maintain stability on the  $x^H$  line in Figure 6 for  $\beta_{\text{eff}}$  values lower than  $\beta_{\text{eff}}^c = 6.97$ . Those supportive connections contribute to the increased region of resilience for the higher graph energies observed in Figure 7(C), the region between  $\beta_{\text{eff}}^c = 6.97$  and where the ecosystems actually start collapsing at  $\beta_{\text{eff},\text{corrected}}^c$ . That offset from the Gao et al. prediction of the tipping point,  $\beta_{\text{eff}}^c$ , could be corrected with a new prediction,  $\beta_{\text{eff},\text{corrected}}^c$ , which is calculated in Section 4.4.

Mutualistic ecosystems tend to have a high degree of nestedness,<sup>59–61</sup> which would result in a more hierarchical structure with lower  $E$ . Some researchers theorize that these natural systems self-optimize around adaptability, more specifically the ability for the ecosystem to evolve so that one species can readily replace another.<sup>62–64</sup> That could lead to higher nestedness and lower  $E$ , potentially resulting in lower precariousness using this method and warranting further study. Another interesting aspect of ecosystems is that their dynamics are difficult to capture because of random changes in behaviors of animals. Consequently, the fit of dynamics equations to an ecosystem's behavior might only be a good fit for a short period of time before that behavior changes. Then, this method might be used to measure the precariousness of the model, perhaps as a measurement of model fitness, instead of the precariousness of the actual ecosystem.

## 4.2 | Case study 2: Supply chain model

For the supply chain case study, the calculation for graph energy was incorporated into the simulations of the randomly generated supply chains from references.<sup>65–66</sup> Using the linearized supply chain dynamics model from Helbing et al.<sup>68</sup>

$$\frac{dn_i}{dt} = x_i(t) - \sum_{j=1}^u c_{ij}x_j(t) - y_i(t) \quad (15)$$

$$\frac{dx_i}{dt} = -An_i(t) - (1+B)x_i(t) + B \sum_{j=1}^u c_{ij}x_j(t) + By_i(t) \quad (16)$$

with the following variables:

- $n_i$ ,  $x_i$ , and  $y_i$  are the linearized deviation from the steady-state inventory, production, and external flow of goods of kind  $i$  with respect to the steady state.
- $c_{ij}$  is an element of the supply matrix  $C$  which is a ratio of the goods of kind  $i$  needed to produce goods of kind  $j$ .
- $A$  is a scalar parameter representing the negative of the partial derivative of the desired production rate with respect to the current inventory.  $A$  is assumed constant across all goods  $i$ .
- $B$  is a scalar parameter representing the negative of the partial derivative of the desired production rate with respect to the current inventory change rate.  $B$  is assumed constant across all goods  $i$ .

The translation of these equations into the effective plane is discussed in Edwards et al.<sup>65</sup> and uses the following conversions:

$$\beta_{\text{eff}} = \frac{\mathbf{1}^T C s^{in}}{\mathbf{1}^T C \mathbf{1}}; x_{\text{eff}} = \frac{\mathbf{1}^T C x}{\mathbf{1}^T C \mathbf{1}}; n_{\text{eff}} = \frac{\mathbf{1}^T C n}{\mathbf{1}^T C \mathbf{1}}; y_{\text{eff}} = \frac{\mathbf{1}^T C y}{\mathbf{1}^T C \mathbf{1}} \quad (17)$$

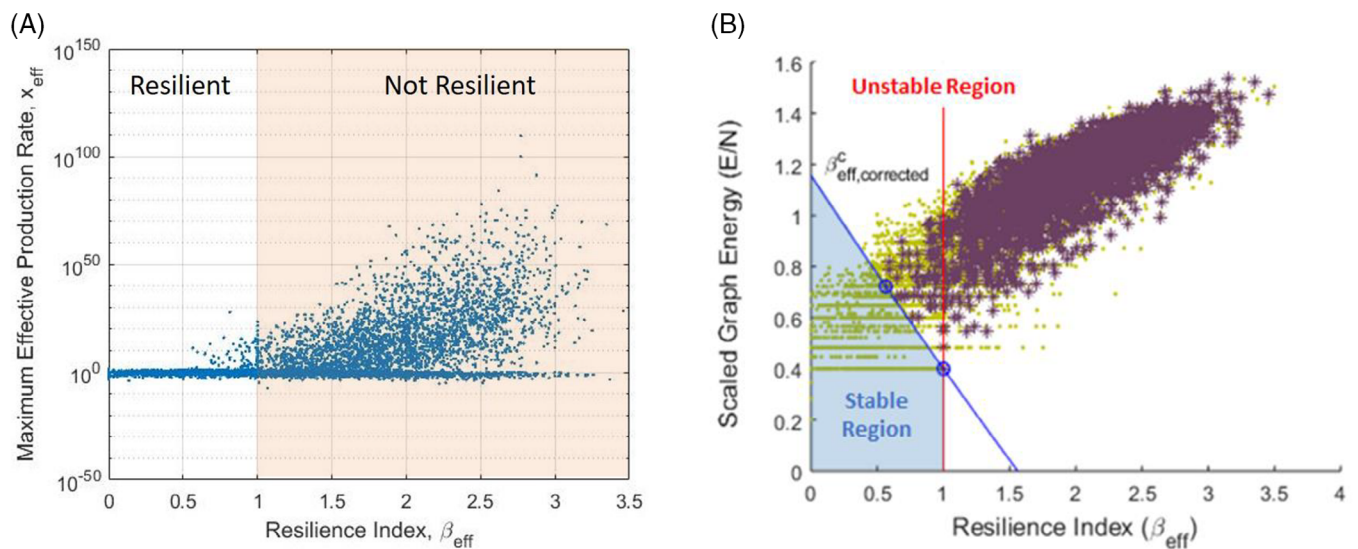


**FIGURE 8** Simulation results (A) and graph energy versus  $\beta_{\text{eff}}$  patterns (B) for supply chain model.

where  $s^{in} = (s_1^{in}, \dots, s_u^{in})^T$  is the vector of incoming weighted degrees in matrix  $\mathbf{C}$ . The translation into the effective plane results in:

$$\frac{dn_{\text{eff}}}{dt} = x_{\text{eff}} - \beta_{\text{eff}}x_{\text{eff}} - y_{\text{eff}} \quad (18)$$

$$\frac{dx_{\text{eff}}}{dt} = -An_{\text{eff}} - x_{\text{eff}} - Bx_{\text{eff}} + B\beta_{\text{eff}}x_{\text{eff}} + By_{\text{eff}} \quad (19)$$

With these equations, the dynamics of the entire network are modeled with two variables that describe the deviation from the steady-state inventory and production in the effective plane ( $n_{\text{eff}}$  and  $x_{\text{eff}}$ ), one driving function ( $y_{\text{eff}}$ ), and two adjustable constants to model the response of all nodes to changing demand and inventory stockpiles (A and B). The stability points of these equations are at  $\beta_{\text{eff}}^c = 1$ , above which the supply chain becomes overloaded with maximized production rates and zeroed inventories.<sup>65</sup>

To validate the model, the simulations for the case study were run with data from the production processes for polystyrene egg trays and recycled egg trays.<sup>66,69</sup> The percentage of reuse for recycled egg cartons was randomly varied as an integer between 0% and 100% and simulated to a distant time of  $t = 1000$  weeks with a MATLAB function ode45 solver.<sup>66</sup> Figure 8 shows the results of 10,000 simulations. Figure 8(A) shows the maximum  $x_{\text{eff}}$ , the weighted sum of the production rates, plotted against  $\beta_{\text{eff}}$ . When  $\beta_{\text{eff}} < 1$ , most of the simulated systems are stable and converge to a low maximum  $x_{\text{eff}}$ . When  $\beta_{\text{eff}} > 1$ , the system behavior bifurcates, with some systems remaining stable but most becoming unstable with a maximum  $x_{\text{eff}}$  diverging to very large numbers. For additional model validation discussion, see.<sup>65,66</sup>

Results from these simulations reveal a similar impact of graph energy on the location of the tipping point as the results from the ecological modeling. Figure 8(B) plots the graph energy,  $E$ , of the binary form of each supply matrix, normalized by the matrix size  $N$ , against its  $\beta_{\text{eff}}$ . Systems that have unstable supply chains are plotted with a mauve

asterisk. Results show when the resilience index is above the predicted tipping point, when  $\beta_{\text{eff}} > 1$ , many of the modeled supply chains could not sustain themselves because they had internal dependencies on reusing more material than they were creating. In this respect,  $\beta_{\text{eff}}$  could be a measure of material conservation in a supply chain. If this model were expanded to include the big data of all internal cycles and external limits for a large complex supply chain, then it could be a powerful tool to detect changes in the data that would lead to resource depletion. Similar to the ecosystem analysis, the region of system instability shifts with the graph energy of the system, and could benefit from a correction like the illustrated  $\beta_{\text{eff}, \text{corrected}}^c$ , which would be a function of  $E$ .

### 4.3 | Case study 3: Disruptive technology model

For the disruptive technology case study, the calculation for graph energy was incorporated into the simulations of the technology markets from reference.<sup>67</sup> The model is adapted from the following predator-prey model from Pielou<sup>70</sup>:

$$\frac{dx_i}{dt} = a_i x_i + b_i x_i^2 - c_i \sum_{j=1}^n A_{ij} x_j x_i \quad (20)$$

Ünver performed a study of technology industry dynamics using this Lotka-Volterra model,<sup>71</sup> in which the disruption of digital cameras in the film-camera industry was simulated. Building on that previous work, the problem can be decomposed into a set of equations, with  $x_1$  representing the units produced with incumbent technology and  $x_2$  representing the units produced with disruptive technology. The adjacency matrix  $A_{ij}$  captures the sales that each technology is taking away from the other. The scalar parameters  $a_i$  and  $b_i$  are used to fit the equations to the data. The scalar parameter  $c_i$  has been added so that the elements  $A_{ij}$  are between 0 and 1, similar to the elements of the

weighted adjacency matrices in the previous two case studies.

$$\frac{dx_1}{dt} = a_1 x_1 + b_1 x_1^2 - c_1 A_{12} x_1 x_2 \quad (21)$$

$$\frac{dx_2}{dt} = a_2 x_2 + b_2 x_2^2 + c_2 A_{21} x_2 x_1 \quad (22)$$

This overall equation in the effective plane can be further decomposed to enable the study of the interactions of different parameters or subsystems. In this case, the behavior of the incumbent ( $x_1$ ) and disruptive ( $x_2$ ) technologies is separated into  $x_{1\text{eff}}$  and  $x_{2\text{eff}}$  to distinguish the interaction between these two parameters. The system is decomposed using the following conversion equations.

$$\beta_{\text{eff}} = \frac{1^T A s^{\text{in}}}{1^T A 1}; x_{1\text{eff}} = \frac{1^T A \begin{bmatrix} x_1 \\ 0 \end{bmatrix}}{1^T A 1}; x_{2\text{eff}} = \frac{1^T A \begin{bmatrix} 0 \\ x_2 \end{bmatrix}}{1^T A 1} \quad (23)$$

resulting in the following equations in the effective plane:

$$\frac{dx_{1\text{eff}}}{dt} = a_1 x_{1\text{eff}} + b_1 x_{1\text{eff}}^2 - c_1 \beta_{\text{eff}} x_{1\text{eff}} x_{2\text{eff}} \quad (24)$$

$$\frac{dx_{2\text{eff}}}{dt} = a_2 x_{2\text{eff}} + b_2 x_{2\text{eff}}^2 + c_2 \beta_{\text{eff}} x_{2\text{eff}} x_{1\text{eff}} \quad (25)$$

with the following stable points:

$$\beta_{\text{eff}}^{c1} = \frac{-2a_1 b_2}{a_2 c_1}; \beta_{\text{eff}}^{c2} = \frac{-2b_1 a_2}{a_1 c_2} \quad (26)$$

The case study simulated was the film-camera disruptive case using the data from Ünver,<sup>71</sup> but with the simplification of  $a = a_1 = a_2 = 0.37$ ,  $b = b_1 = b_2 = -1.6e^{-8}$ , and  $c = c_1 = c_2 = 10e^{-8}$ , which would result in a predicted tipping point of  $\beta_{\text{eff}}^c = \beta_{\text{eff}}^{c1} = \beta_{\text{eff}}^{c2} = -2b/c = 0.32$ . The contents of the weighted adjacency matrix,  $A$ , were randomly generated numbers between 0 and 1. The model was validated with 10,000 simulation runs, with the results shown in Figure 9(A). The  $\beta_{\text{eff}}^c = 0.32$  tipping point line separates the region where the disruptive technology can fail from the region where it will always succeed in attaining a market foothold. The incumbent technology appears to sometimes maintain a market share and sometimes fail in both regions to the left and right of  $\beta_{\text{eff}}^c = 0.32$ . For additional discussion of the model setup and validation, see Nilchiani et al.<sup>67</sup>

In Figure 9(B), the graph energy,  $E$ , for each run is again normalized by the matrix size  $N$ . When the incumbent technology has nonzero sales at the end of the simulation, it is plotted as a dot in the upper plot of Figure 9(B). However, when the incumbent technology is unsuccessful and has zero sales at the end of the simulation, then those results are plotted as a black asterisk, \*, in the upper plot of Figure 9(B). Similarly, when the disruptive technology is successful and has significant sales at the end of the simulation, then the results are plotted as a dot in the lower plot of Figure 9(B). However, when the disruptive technology has less than  $8e^5$  sales, then those results are plotted as a black asterisk in the lower plot of Figure 9(B). The actual tipping point of these systems

is located on the lower edge of the black asterisks in the upper plot and the upper edge of the black asterisks in the lower plot. It is a boundary across which the disruptive technology can go from always succeeding to potentially failing, and the incumbent technology can go from always maintaining a market share to potentially failing. Similar to the previous case studies, the actual tipping point boundary can be defined by a  $\beta_{\text{eff},\text{corrected}}^c$  which shifts away from the predicted tipping point,  $\beta_{\text{eff}}^c$ , as a function of  $E$ .

#### 4.4 | Combined results

Combining the results of each of the case studies, Figure 10 plots  $E$  against  $\beta_{\text{eff}} - \beta_{\text{eff}}^c$ , so that all the graphs have the same tipping-point location at  $\beta_{\text{eff}} - \beta_{\text{eff}}^c = 0$ . While the graphs of the three case studies above normalize graph energy by  $1/N$ , which was theorized to be an appropriate scaling factor by Sinha, Suh, and de Weck,<sup>10</sup> the combined figure below plots  $E$  instead of  $E/N$ . This change was made, because in the derivation of Equation (12) the authors determined that the relationship between  $E$  and  $\beta_{\text{eff}}$  does not have a  $1/N$  factor. When  $E$  is plotted in Figure 10 instead of  $E/N$ , then the data have the same scaling across case studies. The data are labeled with an asterisk (\*) when the system was unstable and transitioned to an undesired state (i.e., the ecosystem collapsed, the supply chain was unsustainable, or the technology failed to gain or maintain a market-hold). The data of the healthy systems (i.e., when the systems maintained their desired state) are not shown in Figure 10(A), because then the figure becomes too cluttered and unreadable. The actual tipping point of the systems, now defined by the line  $\beta_{\text{eff},\text{corrected}} - \beta_{\text{eff}}^c$ , can be fitted along the same tipping-point boundaries in Figure 10 that were first identified in Figures 7–9.

Based on these results, the estimate for the tipping-point location (now defined by the line  $\beta_{\text{eff}}^c - \beta_{\text{eff}}^c = 0$ ) for all systems using this method can be adjusted to slope inversely with graph energy,  $E$ . Assuming an inverse relationship between  $\beta_{\text{eff}}$  and  $E$  (based on the effective system energy Equation (12)), a corrected resilience index  $\beta_{\text{eff},\text{corrected}}^c$  is found using the enveloping edges between stable and unstable regions. A MATLAB script was used to select the data points on the upper edge of the unstable ecosystems and failed disruptive technology, and the lower edge of the unstable supply chains and failed incumbent technology, following the location of the actual tipping points boundaries from Figures 7–9. These data points, circled in (Figure 10A, B), define a combined tipping-point boundary. Then, MATLAB was used to calculate an exponential fit of these points. The results show that increasing the graph energy leads to a greater offset in the system tipping-point threshold, following this exponential curve. This correction, defined by Equation (27), is shown in Figure 10 as a line labeled  $\beta_{\text{eff},\text{corrected}} - \beta_{\text{eff}}^c$ .

$$\beta_{\text{eff},\text{corrected}}^c = \beta_{\text{eff}}^c + \frac{1900}{E + 524} - 3.7 \quad (27)$$

Ultimately, systems engineers who are studying the tipping-points of systems want to either prevent the triggering of an undesired

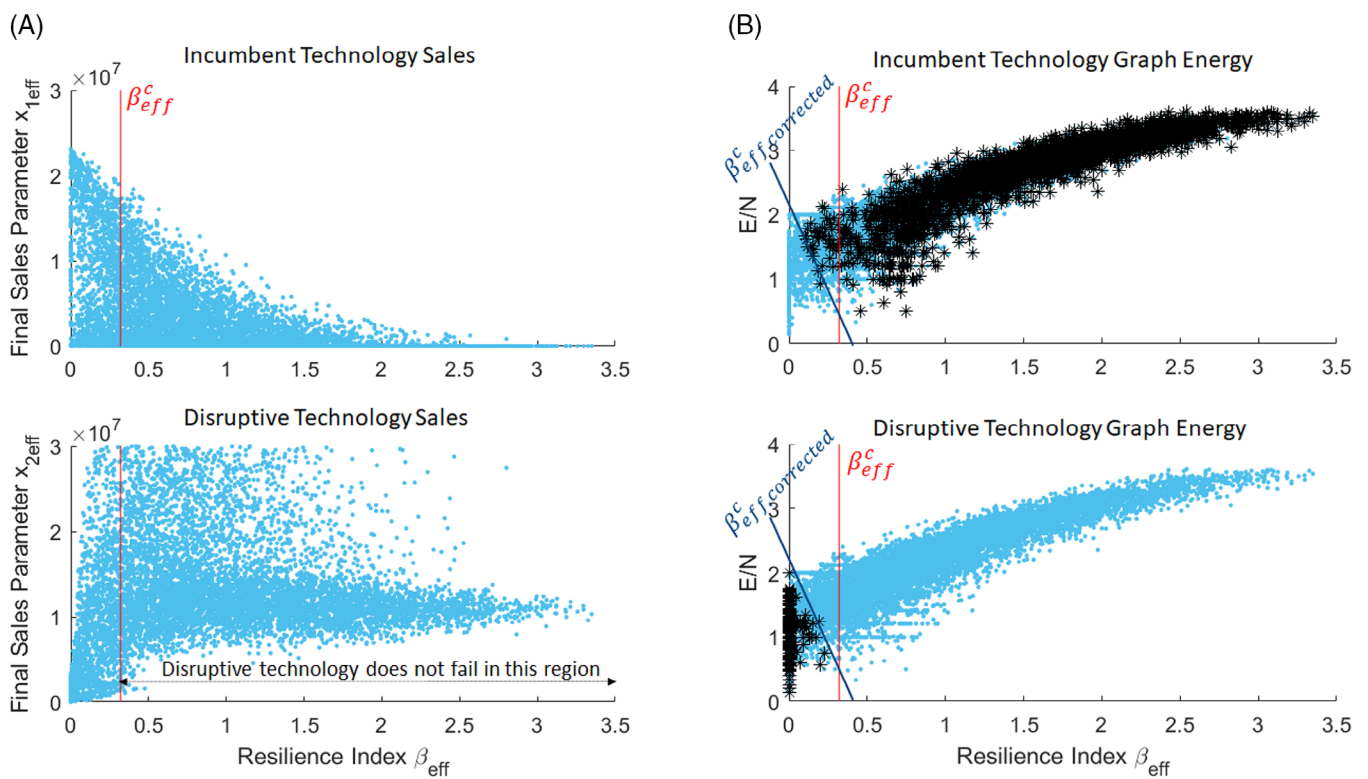


**FIGURE 9** Simulation results (A) and graph energy versus  $\beta_{\text{eff}}$  patterns (B) for disruptive technology model.

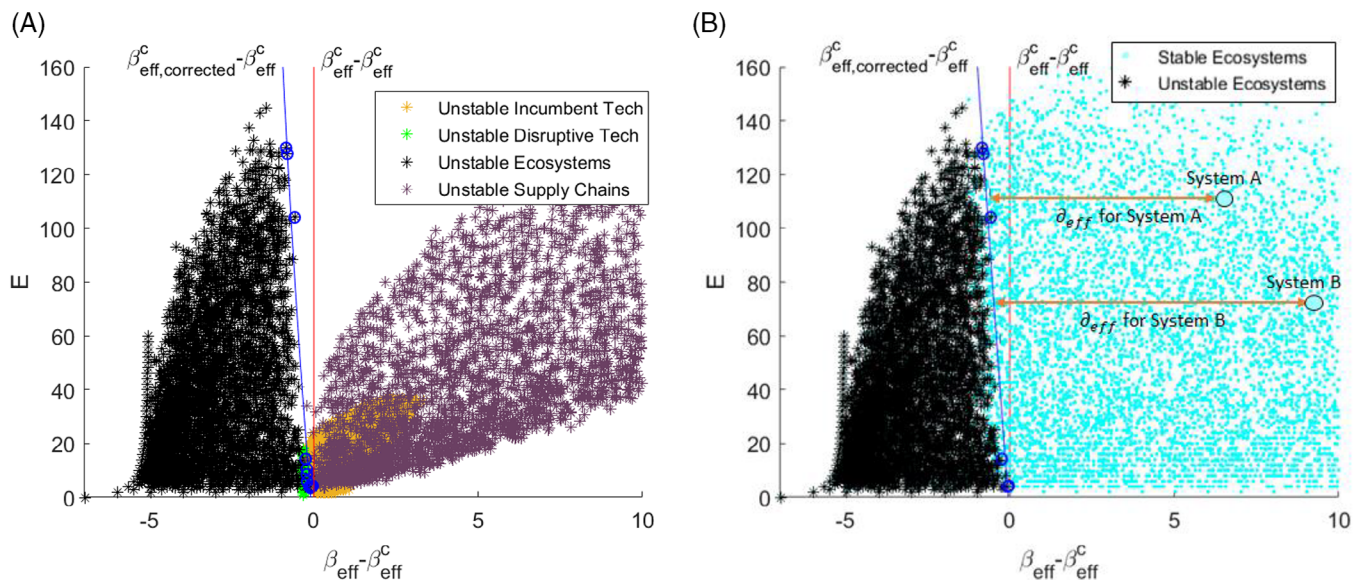


**FIGURE 10** Actual tipping-point boundary ( $\beta_{\text{eff}}, \text{corrected} - \beta_{\text{eff}}^c$ ) shifts away from the predicted tipping point ( $\beta_{\text{eff}}^c - \beta_{\text{eff}}^c = 0$ ) with increasing  $E$  (A) and adjusted resilience index ( $\delta_{\text{eff}}$ ) measures precariousness to that shifted tipping-point boundary (B).

tipping-point, or to control a system through a desired tipping point. To enable this kind of system management, a measurement of precariousness, or how far a system is from a tipping point, is desirable. The adjusted resilience index,  $\delta_{\text{eff}}$  in Equation (28), provides a direct estimate of precariousness, the distance of a system to its tipping points,

and it includes the correction derived in Equation (27). Figure 10(B) illustrates  $\delta_{\text{eff}}$  for two examples of simulated ecosystems. If the method from Gao et al. is used without this correction, then the estimate for precariousness only reaches the  $\beta_{\text{eff}}^c - \beta_{\text{eff}}^c = 0$  line. However, there are systems that maintain stability past that line. The corrected resilience

index,  $\delta_{\text{eff}}$ , adjusts the measurement of precariousness using the new tipping-point boundary  $\beta_{\text{eff},\text{corrected}}^c$  from Equation (27).

$$\delta_{\text{eff}} = \beta_{\text{eff}} - \left( \beta_{\text{eff}}^c + \frac{1900}{E + 524} - 3.7 \right) \quad (28)$$

When the method from Gao et al. is applied to a system modeled as a network, Equation (27) can be applied to incorporate a correction to the location of the predicted tipping point, and Equation (28) can be implemented to calculate the precariousness of how close the system is operating to that tipping point. Returning to the original research questions: (1) does graph energy (as a measurement of topological complexity) affect the accuracy of the resilience index (as a measurement of precariousness), and (2) can topological complexity's impact be measured and integrated into the resilience-index method? Question 1 is answered with Figure 10(A), showing that graph energy does affect the accuracy of the resilience index. Question 2 is achieved with Equation (27) providing a new measurement of that impact and Equation (28) providing a measurement of precariousness that can be integrated into the resilience-index method.

## 5 | CONCLUSION

In summary, this research expanded on a method for a universal resilience index measurement from Gao et al.<sup>11</sup> by introducing a complementary measurement of system topological complexity using graph energy that, when combined, shows how topological complexity impacts the location of tipping points in large-scale systems when modeled as networks. Simulations from case studies in different fields provided data to investigate this relationship. The results answered the overarching research question of whether the complexity of a system affects its resilience to transition or collapse by revealing that the system topological complexity, as measured by graph energy, impacts a system's resilience to tipping points, as measured by the resilience index. That impact was measured, resulting in the introduction of a correction to the resilience index method that adjusts for the topological complexity initially lost in that method's modeling reductions and reveals the location of tipping points with greater accuracy for the measurement and management of system resilience. Also, an adjusted resilience index was introduced that more directly estimates precariousness, the distance of a system to its tipping points.

Overall, this approach can bring new breakthrough insights to domains spanning from mass extinctions to critical infrastructure systems, shedding light on the status of their strength and vulnerability to potential collapse. It provides a means to better understand the tipping points of systems that are so critical to sustain, with a measurement that can be used in system management and risk mitigation to actively avoid or potentially control a system through a tipping point.

## ACKNOWLEDGMENTS

The authors would like to thank Eric Muhle, Kyle Wolma, Karl Strickland, and Amber Bishop for their collaborative efforts in applying

this method to supply chains, which helped to more thoroughly understand its intricacies, strengths, and weaknesses; Todd Sullivan, Vanessa Aponte Williams, Walter Storm, and Ed Danis for championing this work; Prof. Jon Wade at UCSD, Prof. Paul Grogan at ASU, and Prof. Charles Suffel at SIT for their research reviews and feedback; Lockheed Martin for its graduate education support and innovation challenge programs; and the Denver Museum of Nature & Science for its adult education and volunteer programs which helped connect this research with Dr. Ian Miller's work on extinction events.

## DATA AVAILABILITY STATEMENT

NA

## ORCID

Christine M. Edwards  <https://orcid.org/0000-0001-6718-4252>

Roshanak Rose Nilchiani  <https://orcid.org/0000-0002-1488-9934>

## REFERENCES

- Scheffers BR, De Meester L, Bridge TCL, et al. The broad footprint of climate change from genes to biomes to people. *Science*. 2016;354(6313):aaf7671.
- Donohue I, Hillebrand H, Montoya JM, et al. Navigating the complexity of ecological stability. *Ecol Lett*. 2016;19(9):1172-1185.
- Mitra C, Choudhary A, Sinha S, Kurths J, Donner RV. Multiple-node basin stability in complex dynamical networks. *Phys Rev E*. 2017;95(3):032317.
- Linkov I, Trump BD, Fox-Lent K. Resilience: approaches to risk analysis and governance. *IRGC Resource Guide on Resilience*. International Risk Governance Center; 2016.
- Holling CS. In: Schultz PC, ed. *Engineering Resilience versus Ecological Resilience Engineering within Ecological Constraints*. National Academy Press; 1996.
- Hodgson D, McDonald JL, Hosken DJ. What do you mean 'resilient'? *Trends Ecol Evol*. 2015;30(9):503-506.
- Madni AM, Jackson S. Towards a conceptual framework for resilience engineering. *IEEE Syst J*. 2009;3(2):181-191.
- Ayyub BM. Systems resilience for multihazard environments: definition, metrics, and valuation for decision making. *Risk Anal*. 2014;34(2):340-355.
- Deangelis DL. Energy flow, nutrient cycling, and ecosystem resilience. *Ecology*. 1980;61(4):764-771.
- Solé RV, Montoya M. Complexity and fragility in ecological networks. *Proc R Soc London B*. 2001;268(1480):2039-2045.
- Gao J, Barzel B, Barabási A-L. Universal resilience patterns in complex networks. *Nature*. 2016;530(7590):307-312.
- Sinha K, Suh ES, De Weck O. Integrative complexity: an alternative measure for system modularity. *J Mech Des*. 2018;140(5):051101.
- Pugliese A, Nilchiani R. Developing spectral structural complexity metrics. *IEEE Syst J*. 2019;13(4):3619-3626.
- Graovac A, Gutman I, Trinajstić N. *Topological approach to the chemistry of conjugated molecules*. Springer; 1977.
- Gutman I, Polansky OE. *Mathematical concepts in organic chemistry*. Springer; 1986.
- Trinajstić N. *Chemical graph theory*. Routledge; 1983.
- Dias JR. *Molecular orbital calculations using chemical graph theory*. Springer-Verlag; 1993.
- Hückel E. Quantentheoretische beiträge zum benzolproblem. *Zeitschrift für Physik*. 1931;72(5):310-337.

19. Gutman I, Furtula B. The total  $\pi$ -electron energy saga. *Croat Chem Acta*. 2017;90(3):1-10.
20. Hückel E. Grundzüge der Theorie ungesättigter und aromatischer Verbindungen. *Zeitschrift für Elektrochemie und angewandte physikalische Chemie*. 1937;43(9):752-788.
21. Coulson CA, O'Leary B, Mallion RB. *Hückel theory for organic chemists*. Academic Pr; 1978.
22. Rakshit SC, Hazra B. Correlations among molecular-properties, quantum-mechanical and topological quantities. *J Indian Chem Soc*. 1990;67(11):887-891.
23. Gutman I, Vidovic D, Cmiljanovic N, Milosavljevic S, Radenkovic S. Graph energy-a useful molecular structure-descriptor. *Indian J Chem A: Inorgan Phys Theor Anal*. 2003;42(6):1309-1311.
24. Dehmer M, Li X, Shi Y. Connections between generalized graph entropies and graph energy. *Complex*. 2015;21(1):35-41.
25. Li X, Qin X, Wei M, Gutman I, Dehmer M. Novel inequalities for generalized graph entropies-graph energies and topological indices. *Appl Math Comput*. 2015;259:470-479.
26. Wu H, Zhang Y, Chen W, Mu Z. Comparative analysis of protein primary sequences with graph energy. *Phys A*. 2015;437:249-262.
27. Di Paola L, Mei G, Di Venere A, Giuliani A. Exploring the stability of dimers through protein structure topology. *Curr Protein Pept Sci*. 2016;17(1):30-36.
28. Sheard SA, Mostashari A. A complexity typology for systems engineering. *INCOSE International Symposium*. 2010;20(1):933-945.
29. Sillitto HG. On Systems Architects and Systems Architecting: some thoughts on explaining and improving the art and science of systems architecting. *INCOSE International Symposium*. 2009;19(1):970-985.
30. Wade J, Heydari B. Complexity: definition and reduction techniques. *Proceedings of the Poster Workshop at the 2014 Complex Systems Design & Management International Conference*; 2014.
31. ESD Symposium Committee, *ESD Terms and Definitions Version 16*. Massachusetts Institute of Technology Engineering Systems Division; 2007.
32. Strogatz S. *SYNC-The emerging science of spontaneous order*. Penguin; 2004.
33. Phelan SE. What is complexity science, really? *Emergence, J Complex Issues Organiz Manage*. 2001;3(1):120-136.
34. Lloyd S. *Measures of complexity: a non-exhaustive list*. d'Arbeloff; 2009.
35. Fischl J, Nichiani R. Complexity based risk evaluation in engineered systems. *Proc Comput Sci*. 2015;44:31-41. ed. C.
36. Shannon CE. A mathematical theory of communication. *Bell Syst Tech J*. 1948;27(3):379-423.
37. Willcox K, et al. *Stochastic process decision methods for complex-cyber-physical systems*. Massachusetts Institute of Technology; 2011.
38. Allen EB. Measuring graph abstractions of software: an information-theory approach. *Proceedings Eighth IEEE Symposium on Software Metrics*. IEEE; 2002.
39. McCabe TJ. A complexity measure. *IEEE Trans Software Eng*. 1976;4:308-320.
40. Nikiforov V. The energy of graphs and matrices. *J Math Anal Appl*. 2007;326(2):1472-1475.
41. Stankovic A. The definition and quantification of resilience. *IEEE PES Industry Technical Support Task Force*. IEEE; 2018.
42. Grid resilience in regional transmission organizations and independent system operators. FERC Docket No. AD18-7-000; 2018.
43. Walker B, Holling CS, Carpenter SR, Kinzig AP. Resilience, adaptability and transformability in social-ecological systems. *Ecol Soc*. 2004;9(2):5-9.
44. Holling CS. Engineering resilience versus ecological resilience. *Eng Ecol Constraints*. 1996;31:32.
45. Allen CR, Garmestani AS, Sundstrom S, Angeler DG. Ecological resilience. In: Florin MV, Linkov I, eds. *IRGC resource guide on resilience*. EPFL International Risk Governance Center (IRGC); 2016:15-18.
46. Dakos V, Kéfi S. Ecological resilience: what to measure and how. *Environ Res Lett*. 2022;17(4):043003.
47. Nolting BC, Abbott KC. Balls, cups and quasi-potentials: quantifying stability in stochastic systems. *Ecology*. 2016;97:850-864.
48. Hastings A, Wysham DB. Regime shifts in ecological systems can occur with no warning. *Ecol Lett*. 2010;13:464-472.
49. Van Nes EH, Arani BMS, Staal A, et al. What do you mean, 'tipping point'? *Trends Ecol Evol*. 2016;31(12):902-904.
50. Solé RV, Manrubia SC, Luque B, Delgado J, Bascompte J. Phase transitions and complex systems: simple, nonlinear models capture complex systems at the edge of chaos. *Complex*. 1996;1(4):13-26.
51. van Voorn GA. *Tipping points in natural systems. An inventory of types, early warnings, and consequences*. Wageningen University; 2012.
52. Novak M, Yeakel JD, Noble AE, et al. Characterizing species interactions to understand press perturbations: what is the community matrix? *Annu Rev Ecol Evol Syst*. 2016;47:409-432.
53. Fuller EC, Samhouri JF, Stoll JS, Levin SA, Watson JR. Characterizing fisheries connectivity in marine social-ecological systems. *ICES J Mar Sci*. 2017;74(8):2087-2096.
54. Biamonte J, Faccin M, De Domenico M. Complex networks: from classical to quantum. *Commun Phys*. 2019;2(1):1-10.
55. Mitra C, Choudhary A, Sinha S, Kurths J, Donner RV. Multiple-node basin stability in complex dynamical networks. *Phys Rev E*. 2017;95(3):032317.
56. Alcaraz C. Cloud-assisted dynamic resilience for cyber-physical control systems. *IEEE Wirel Commun*. 2018;25(1):76-82.
57. Jiang J, Huang Zi-G, Seager TP, et al. Predicting tipping points in mutualistic networks through dimension reduction. *Proc Natl Acad Sci USA*. 2018;115(4):E639-E647.
58. Tu C, Grilli J, Schuessler F, Suweis S. Collapse of resilience patterns in generalized Lotka-Volterra dynamics and beyond. *Phys Rev E*. 2017;95(6):062307.
59. Bascompte J, Jordano P, Melián CJ, Olesen JM. The nested assembly of plant-animal mutualistic networks. *Proc Natl Acad Sci*. 2003;100(16):9383-9387.
60. Mariani MS, Ren Z-M, Bascompte J, Tessone CJ. Nestedness in complex networks: observation, emergence, and implications. *Phys Rep*. 2019;813:1-90.
61. Chatterjee A, Brehm C, Layton A. Evaluating benefits of ecologically-inspired nested architectures for industrial symbiosis. *Resour Conserv Recycl*. 2021;167.
62. Ulanowicz RE. The dual nature of ecosystem dynamics. *Ecol Model*. 2009;220(16):1886-1892.
63. Chatterjee A, Malak R, Layton A. Ecology-inspired resilient and affordable system of systems using degree of system order. *Syst Eng*. 2022;25(1):3-18.
64. Fath BD. Quantifying economic and ecological sustainability. *Ocean Coast Manage*. 2015;108:13-19.
65. Edwards CM, Muhle E, Wolma K, Bishop A, Nilchiani RR. Identification of tipping points in supply chain dynamics using effective dimension and resilience index. *2018 Annual IEEE International Systems Conference (SysCon)*. IEEE; 2018.
66. Edwards CM, Nilchiani RR, Wade J, Strickland K. Reuse optimization and tipping-point resilience in supply chains. *2019 IEEE International Systems Conference (SysCon)*. IEEE; 2019.
67. Nilchiani R, Edwards CM, Ganguly A. Introducing a tipping point measure in explaining disruptive technology. *2019 International Symposium on Systems Engineering (ISSE)*. IEEE; 2019.
68. Helbing D, Lämmer S, Seidel T, Šeba P, Piątkowski T. Physics, stability, and dynamics of supply networks. *Phys Rev E*. 2004;70(6):066116.
69. Ocampo L, Carreon R, Carvajal JA, Galagar KJ, Gialolo DM, Gulayan M, Indig D, Nunez DM, Tagsip WC, Vallecera JM, Villegas Z. Matrix-based

- life cycle assessment (MLCA) on polystyrene and recycled paper egg tray packaging. *J Prod Eng.* 2015;18(1):87-91.
70. Pielou EC. *An introduction to mathematical ecology*. Wiley-Interscience; 1969.
71. Ünver HÖ. A comparative study of Lotka-Volterra and system dynamics models for simulation of technology industry dynamics. Ph.D. dissertation, Massachusetts Institute of Technology; 2008.

**How to cite this article:** Edwards CM, Nilchiani RR, Miller IM.

Impact of graph energy on a measurement of resilience for tipping points in complex systems. *Systems Engineering*. 2024;27:745-758. <https://doi.org/10.1002/sys.21749>